Efficient quasi-kinematic large-scale dynamo as the small-scale dynamo saturates

Pallavi Bhat*

Plasma Science and Fusion Center, Massachusetts Institute of Technology, Cambridge, MA 02139, USA and
Department of Applied Mathematics, University of Leeds, Leeds, LS2 9JT, UK

Kandaswamy Subramanian

IUCAA, Post Bag 4, Ganeshkhind, Pune 411007, India

Axel Brandenburg

Nordita, KTH Royal Institute of Technology and Stockholm University, SE-10691 Stockholm, Sweden
Department of Astronomy, AlbaNova Center, Stockholm University, SE-10691 Stockholm, Sweden
JILA and Laboratory for Atmospheric and Space Physics, University of Colorado, CO 80303, USA and
McWilliams Center for Cosmology & Department of Physics, Carnegie Mellon University, PA 15213, USA
(Dated: May 22, 2019, Revision: 1.63)

Large-scale magnetic fields in stars and galaxies are thought to arise by mean-field dynamo action due to the combined influence of both helical turbulence and shear. Those systems are also highly conducting and the turbulence therein leads to a fluctuation (or small-scale) dynamo which more rapidly amplifies magnetic field fluctuations on the eddy scales and smaller. Will this then interfere with and suppress the mean (or large-scale) field growth? Using direct numerical simulations of helical turbulence (with and without shear), we identify a novel quasi-kinematic large-scale dynamo which operates as the small-scale dynamo saturates. Thus both dynamos operate efficiently, one after the other, and lead to the generation of significant large-scale fields.

Magnetic fields coherent on large-scales, larger than the scales of turbulent motions in the system, are prevalent in stars and disk galaxies. Their origin is thought to lie in mean-field or large-scale dynamo (LSD) action due to helical turbulence often combined with shear. Turbulence in stars and galaxies also has a very high magnetic Reynolds number R_M. This generically leads to a fluctuation or small-scale dynamo (SSD) which grows random and small-scale magnetic fields more rapidly [1, 2]. Here, small scales correspond to scales smaller than the outer scale of the turbulence. A question of outstanding importance is whether these two dynamos (LSD and SSD) cooperate or compete with each other in the presence of rapidly growing fluctuations [3]. Moreover, can we see evidence of both dynamos in a large R_M system?

Earlier work using direct numerical simulations showed that helically forced turbulence at large R_M acts as a unified dynamo in the kinematic stage and grows magnetic fields, of both large and small scales, with a shape-invariant eigenfunction [4, 5]. It is also known that saturation of the dynamo occurs first at small scales, and then at progressively larger scales. Thus, the field at scales larger than the forcing scale of the turbulence continues to grow even when the field at smaller scales has already saturated [5]. Eventually, the large-scale field goes into the growth phase governed by the resistive decay of small-scale helicity [6]. In this work, we use helically forced turbulence with uniform shear (and sometimes without) to identify a novel intermediate second stage of exponentially growing large-scale field, different from that of the kinematic unified dynamo, due to a quasi-kinematic LSD.

This arises in a previously unexplored parameter regime, but one that is in fact expected to be generic.

We have run direct numerical simulations (DNS) of forced weakly compressible turbulence solving the magnetohydrodynamics (MHD) equations in a periodic or shearing-periodic cube of size L^3 with $L = 2\pi$, so the smallest wavenumber is $k_1 = 2\pi/L = 1$. We follow a setup similar to that of Ref. [5], except now we also have cases with uniform linear shear. The simulations were performed with the PENCIL CODE [7], and have a resolution of 512^3 and a magnetic Prandtl number of $P_M = 10$. We have specified the relevant parameters for each run in Table I. Turbulence is driven at the forcing wave number of $k_f/k_1 = 4$ (or 8 in one case). In our DNS, the unit of velocity is the sound speed c_s, and that of time is $(c_s k_1)^{-1}$. Our two main runs – one with shear (Run A) and one without shear (Run B) – have helical forcing which can lead to LSD action. In the following, we discuss results from these runs and compare with two similar runs (C and D) with non-helical forcing and thus only SSD action.

In the top panels of Figs. 1 and 2, we show the evolution of the magnetic energy spectrum M_k at certain wave numbers k. We characterize large- and small-scale fields through the magnetic energy at $k < k_f$ and $k > k_f$, respectively. The quantity M_1 is seen to grow exponentially at the same kinematic rate as others until about $t = 100$. However, there is a second phase between $t = 100$ to $t \sim 250$–270, where M_1 grows exponentially at a different, albeit slower rate. Meanwhile all modes with $k \geq k_f$ have slowed down towards saturation. In a third phase, after $t \sim 300$, the growth of M_1 further slows down to a resistively limited rate. For Run A, we have also calculated the large-scale field $\overline{B}_{\rm rms}$ from horizontal or xy
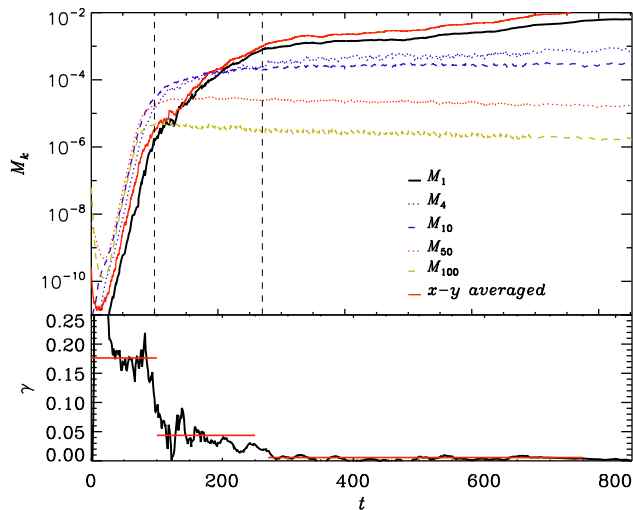
---
* P.Bhat@leeds.ac.uk

FIG. 1. Evolution of $M_k(t)$ for $k = 1, 4, 10, 50,$ and 100 for Run A. Evolution of energy in xy averaged field $\overline{\boldsymbol{B}}_{\mathrm{rms}}^2$ in solid red. The bottom panel shows γ, the growth rate of M_1.

FIG. 2. Evolution of $M_k(t)$ for $k = 1, 4, 10, 50,$ and 100 has been shown for Run B.

averaging. In the top panel of Fig. 1, we show that evolution of $\overline{\boldsymbol{B}}_{\mathrm{rms}}^2$ closely follows the M_1 curve. Thus, the three different phases of growth are observed also in the evolution of the large-scale field calculated from this different method. In the bottom panels of Figs. 1 and 2, we plot the growth rate of M_1, defined as $\gamma = d\ln(M_1)/dt$. Three stages of growth can clearly be identified.

We propose that this second distinctive phase of growth of the large-scale field is in fact a standard LSD – as predicted by mean-field dynamo theory. In the first stage, which is entirely kinematic, the faster SSD is the main driver and thus governs the growth rate of magnetic energy over all scales. The large-scale field at $k = 1$ grows as a low wave number tail of the SSD eigenfunction, coupled to the small scales, possibly through a $k^{3/2}$ [1, 2] or a $k^{7/6}$ [4] slope. Once the growth at smaller scales has slowed down, large-scale dynamo action becomes prominent.

For the following discussion, it is helpful to refer to the standard mean-field equations obtained by splitting the induction equation into one for the mean or large-scale field $\overline{\boldsymbol{B}}$ and the fluctuating or small-scale field $\boldsymbol{b}$ [8],

$$\frac{\partial \overline{\boldsymbol{B}}}{\partial t} = \boldsymbol{\nabla} \times \left(\overline{\boldsymbol{U}} \times \overline{\boldsymbol{B}} + \boldsymbol{\mathcal{E}} - \eta \boldsymbol{\nabla} \times \overline{\boldsymbol{B}} \right), \qquad (1)$$

$$\frac{\partial \boldsymbol{b}}{\partial t} = \boldsymbol{\nabla} \times \left(\overline{\boldsymbol{U}} \times \boldsymbol{b} + \boldsymbol{u} \times \overline{\boldsymbol{B}} - \eta \boldsymbol{\nabla} \times \mathbf{b} + \mathbf{G} \right). \qquad (2)$$

Here $\boldsymbol{\mathcal{E}} = \overline{\boldsymbol{u} \times \boldsymbol{b}}$ and $\boldsymbol{G} = \boldsymbol{u} \times \boldsymbol{b} - \boldsymbol{\mathcal{E}}$ is a term nonlinear in the fluctuations. The mean velocity accounts for the linear shear, $\overline{\boldsymbol{U}} = (0, Sx, 0)$, where $S = $ const. We also find that helical forcing combined with shear induces a large-scale flow $\overline{\boldsymbol{U}} = (\overline{U}_x(z), \overline{U}_y(z), 0)$ on xy averaging but this does not appear to affect the LSD (see below).
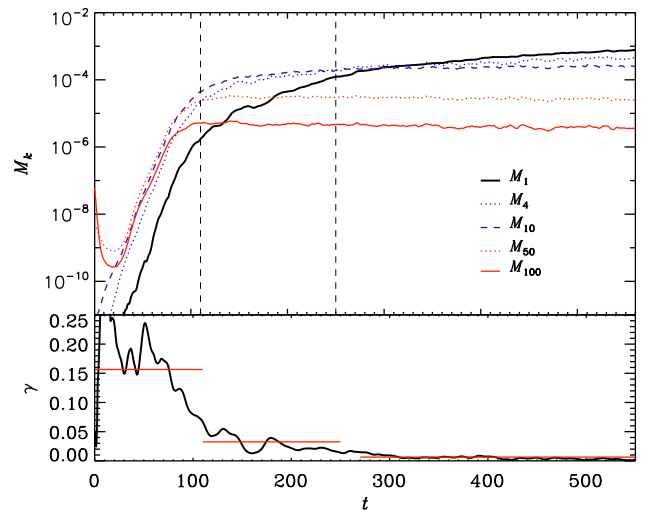
This phenomenon is the vorticity dynamo [9, 10], which is known to be suppressed by the magnetic field [11, 12].

During the kinematic stage, the small-scale field is mainly driven by $\boldsymbol{\nabla} \times (\boldsymbol{u} \times \boldsymbol{b})$, which leads to SSD action. All the terms that depend on averaged or mean quantities are not significant initially. We have checked that the shear in our simulations is small enough that its effect on SSD growth is unimportant [13]. The small-scale field then grows exponentially as $\boldsymbol{b} = \boldsymbol{b}_0 \exp(\gamma_{\mathrm{SSD}}t)$, where γ_{SSD} is the SSD growth rate. In Eq. (1), the time evolution of $\boldsymbol{\mathcal{E}}$, which drives $\overline{\boldsymbol{B}}$, is then controlled by the exponentially growing low wave number tail of the small-scale field, given that the velocity field $\boldsymbol{u}$ is in statistical steady state. The shear term $\boldsymbol{\nabla} \times \left(\overline{\boldsymbol{U}} \times \overline{\boldsymbol{B}} \right)$ is subdominant as $\overline{\boldsymbol{B}}$ is at this stage much smaller than $\boldsymbol{b}$. The rate of change of $\overline{\boldsymbol{B}}$ is therefore expected to be nearly the same as γ_{SSD}. This can be seen also in Fig. 3, where in the left panel we show that the time evolution of M_1 in both the helical shear dynamo simulations (Run A) and non-helical shear dynamo (Run C) coincide in the kinematic stage. Similarly, in the right panel of Fig. 3, the M_1 curves from helical dynamo (Run B) and non-helical dynamo (Run D) coincide. Thus, the kinematic stage is primarily driven by the SSD with $\overline{\boldsymbol{B}}$ being enslaved to $\boldsymbol{b}$.

Eventually, the growth of the small-scale field slows down from an exponential to a more linear form as the SSD begins to saturate. We find this coincides with a second stage of exponential growth of the large-scale field. As seen in the upper panel of Fig. 1, the evolution of M_4 and field at even smaller scales M_{10}, slow down at around $t = 100$, when M_1 switches to a different rate of exponential growth. Figure 4 shows explicitly the exponentially growing M_1 versus linearly growing M_4, from Run A. We can understand the second stage of growth of the large-scale field in the following manner. In Eq. (2), besides the shear and SSD terms, now there are contri-
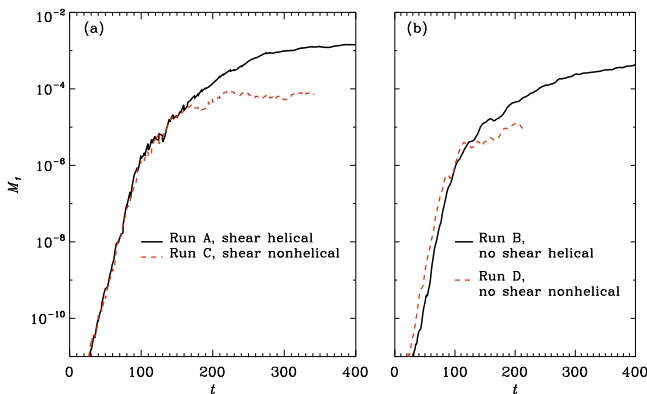
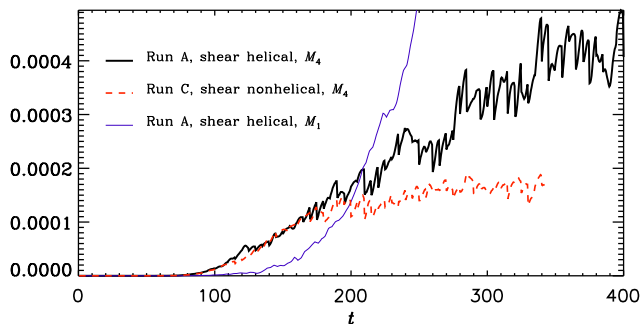FIG. 3. Comparison of M_1 curves between Runs A and C in the panel (a) and between Runs B and D in the panel (b).

FIG. 4. Comparison of $M_4(t)$ shown for Run A and Run C. Also comparison of curves from Run A – M_1 growing exponentially while M_4 grows linearly.

butions due to the terms containing mean quantities. In particular, the term $\boldsymbol{\nabla} \times (\boldsymbol{u} \times \overline{\boldsymbol{B}})$, interpreted as the tangling of the large-scale field, is expected to be responsible for additional growth of small-scale fields over and above that when there is no large-scale dynamo. We show that this is indeed the case in Fig. 4, where the linear growth rate of the M_4 in the helical dynamo in Run A is larger than that of non-helical dynamo (Run C) by a factor of about 8.

At this stage, as the tangling of large-scale field by the random velocity $\boldsymbol{u}$ becomes the more dominant mecha-

TABLE I. Summary of all the runs.

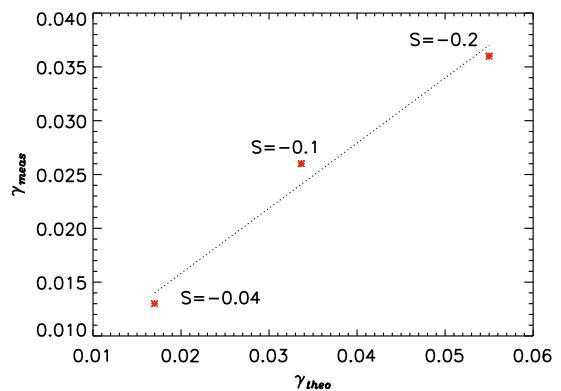| Run	k_{f}	u_{rms}	$S\tau$	forcing	R_M	γ_{theo}	γ_{meas}
A	4	0.13	0.38	helical	812	0.055	0.036
B	4	0.18	0	helical	1062	0.060	0.032
C	4	0.13	0.38	non-hel	812	–	–
D	4	0.19	0	non-hel	1187	–	–
E	4	0.10	0.25	helical	1000	0.033	0.026
F	4	0.09	0.11	helical	812	0.017	0.013
G	8	0.09	0.27	helical	281	0.051	0.032
H	4	0.18	0	helical	531	0.06	0.034

FIG. 5. Comparison between theoretical $\gamma_{\mathrm{theo}} = -\eta_{\mathrm{T}} k^2 \pm |\frac{1}{2}\alpha S k_z|^{1/2}$ and measured $\gamma_{\mathrm{meas}} = d\ln M_1/dt$, for Runs A, E and F (with varying shear, S).

nism for growth of small-scale fields $\boldsymbol{b}$, this leads to a correlation between $\boldsymbol{b}$ and $\boldsymbol{u}$, proportional to $\overline{\boldsymbol{B}}$. The emf $\boldsymbol{\mathcal{E}} = \overline{\boldsymbol{u} \times \boldsymbol{b}}$, which then depends on $\overline{\boldsymbol{B}}$, can be estimated by the usual closure scheme, first order smoothing approximation (FOSA), to be $\boldsymbol{\mathcal{E}} = \alpha\overline{\boldsymbol{B}} - \eta_{\mathrm{t}}\boldsymbol{\nabla} \times \overline{\boldsymbol{B}}$ [8]. Here α and η_{t} are the turbulent transport coefficients determining the effect of small-scale turbulence on the large-scale magnetic field. Thus, Eq. (1) for the large-scale field transforms to,

$$\frac{\partial \overline{\boldsymbol{B}}}{\partial t} = \boldsymbol{\nabla} \times \left(\overline{\boldsymbol{U}} \times \overline{\boldsymbol{B}} + \alpha\overline{\boldsymbol{B}}\right) + \eta_{\mathrm{T}}\nabla^2\overline{\boldsymbol{B}}, \quad \boldsymbol{\nabla} \cdot \overline{\boldsymbol{B}} = 0, \quad (3)$$

with $\eta_{\mathrm{T}} = \eta + \eta_{\mathrm{t}}$. This is the standard mean-field dynamo equation, which has solutions in a periodic box of the form $\overline{\boldsymbol{B}}(\boldsymbol{x}, t) = \mathrm{Re}\left[\hat{\boldsymbol{B}}(\boldsymbol{k})\exp(i\boldsymbol{k}\cdot\boldsymbol{x} + \lambda t)\right]$ at the kinematic stage. For simplicity assume the large-scale field varies only along z and so $k_y = k_x = 0$. Then the eigenvalue λ is given by [14],

$$\lambda_\pm = -\eta_{\mathrm{T}} k_z^2 \pm (\alpha^2 k_z^2 - i\alpha S k_z)^{1/2}. \quad (4)$$

We note that the $\overline{\boldsymbol{U}}$ from the vorticity dynamo does not affect the dispersion relation as $\boldsymbol{\nabla} \times (\overline{\boldsymbol{U}} \times \overline{\boldsymbol{B}}) = 0$ when $\overline{B}_z = \overline{U}_z = 0$ and the fields depend only on z. For Run A, the vorticity dynamo becomes suppressed as the magnetic field continues to saturate [15].

For the case without shear (α^2 dynamo), the growing mode has $\lambda = |\alpha|k_z - \eta_{\mathrm{T}} k_z^2$. When shear dominates (standard $\alpha\Omega$ dynamo), such that $\alpha k_z/S \ll 1$,

$$\mathrm{Re}\lambda_\pm \approx -\eta_{\mathrm{T}} k_z^2 \pm |\frac{1}{2}\alpha S k_z|^{1/2}, \quad (5)$$

$$\mathrm{Im}\lambda_\pm \equiv -\omega_{\mathrm{cyc}} \approx \pm|\frac{1}{2}\alpha S k_z|^{1/2}. \quad (6)$$

We now ask, can the second stage of exponential growth of $\overline{\boldsymbol{B}}$ shown in Fig. 1, be understood in terms of the above standard mean-field dynamo properties? For homogeneous, isotropic and fully helical turbulence
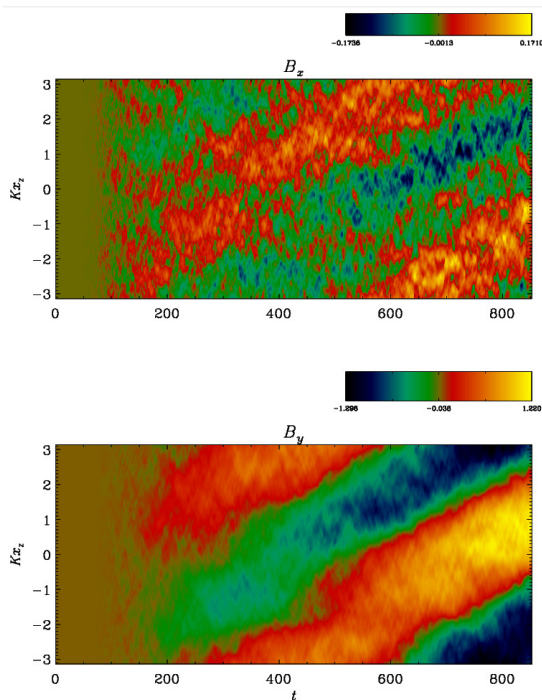
FIG. 6. Space-time diagram where the field components have been xy averaged.

forced at a wave number k_f, we estimate $\alpha \sim u_{rms}/3$ and $\eta_t \sim u_{rms}/(3k_f)$ [16]. The second term (with shear) in Eq. (5) governs the growth rate, while the first term would be smaller in the supercritical case. In our Run A, $u_{rms} \sim 0.13$, $k_f = 4$ and $S\tau \sim 0.38$, which leads to $\gamma_{theo} = \text{Re}\lambda_+ \sim 0.055$, which is larger than the measured value of $\gamma_{meas} \sim 0.036$. This yields an 'efficiency factor' $c_{effic} \sim 0.65$. Note that in the runs with shear, we estimate the u_{rms} after subtracting out $\overline{U}$.

From Eq. (5), we observe that the growth rate is not expected to change much as we change k_f. We have run a case with $k_f = 8$, where $u_{rms} \sim 0.09$ and $S\tau \sim 0.27$, yielding $\gamma_{theo} \sim 0.051$. This theoretical estimate is similar to the γ_{theo} of Run A. This is also confirmed by the measurement of the growth rate of ~ 0.032 (similar to measured value of 0.036 in Run A). In the no-shear case, the theoretical growth rate estimate is given by $u_{rms}k_f/12$. For Run B, where $u_{rms} \sim 0.18$ this leads to $\gamma_{theo} \sim 0.06$. Here, with $\gamma_{meas} \sim 0.032$, we have $c_{effic} \approx 0.53$.

We have varied the shear parameter $S\tau$ to see its effect on this second stage growth rate of the large-scale field. In Fig. 5, we compare the theoretical estimate of the growth rate for the Runs A, E and F (with different values of the shear parameter) against the measured value. We find that c_{effic} is roughly the same in all three cases, thus leading to the points in Fig. 5 falling nearly on a straight line.

Next we examine the oscillatory behavior of the LSD in the runs with shear. In Fig. 6, we show xy averaged fields $\overline{B}_x$ and $\overline{B}_y$ in a zt space-time diagram. As in earlier work

at lower R_M [11], the oscillations begin only during the second stage of growth of the large-scale field. We make a theoretical estimate of the time period of this cycle from the mean-field theory. If we take $\text{Re}\lambda_+$ in Eq. (5) to 0 (which approximately holds as the LSD saturates), we obtain $\omega_{cyc} = \eta_T k_z^2$. Thus, the time period can written as $T = 2\pi/\omega_{cyc} = 6\pi(k_f/k_1)^2$. For Run A, such an estimate yields $T \sim 300$ and we find from the simulation shown in Fig. 6, this is roughly the time period of the oscillations in the large-scale field. From these results, it appears that the mean-field theory is satisfactorily applicable to understand the LSD in this second stage.

An important question is whether there are any effects due to varying R_M on the large-scale field growth in this stage? To check this we have lowered in Run H the R_M by a factor of 2 compared to that of Run B. We find that the growth rate in this Run H is indeed the same as that in Run B. Lastly, the third stage of slow growth of the large-scale field is governed by the resistive decay of small-scale magnetic helicity, which had built up to suppress the α-effect, as shown by previous works [6, 14, 17, 18]; see also [19]. At late times, there could also be a fourth phase of nonlinear mode switching of the helical dynamo when linear shear is included [20]; see also [21].

Our earlier simulation of the helical LSD [5], also at $\text{P}_M = 10$, had a higher resolution (1024^3) but a smaller $u_{rms} \sim 0.12$. Thus, the resulting growth rate $u_{rms}k_f/12$ of the LSD was small and thus it was difficult to delineate the second stage from the third stage where growth is governed by resistive effects. It is important to recognize that our simulations are in a parameter regime which allows for separation in large-scale field growth time scales between the three stages. This made it possible to identify the second stage here. Also such a separation in growth time scales can be expected in astrophysical systems. A suggestion of an intermediate stage of LSD growth was made earlier [22], but did not receive much emphasis then. Also, this was a very different system with convection and boundaries permitting a magnetic helicity flux.

A caveat in our estimates is that we are applying mean-field theory to a system which is already affected by the Lorentz force (as the SSD slows down) and thus the theory needs to include the nonlinear effects. However, it may be possible that the nonlinearity affects only the small-scale fields at this stage, while the theory for the large-scale field, involving an effective α effect could still be applicable and thus we term it a quasi-kinematic LSD. It has been suggested that the spatial intermittency of the magnetic field when SSD saturates could still allow the LSD to operate [23]. Note that the quasi-kinematic LSD here arises upon saturation of the SSD and seems to be in alignment with the 'suppression principle' put forward by Tobias and Cattaneo [24], although there the SSD is suppressed even in the kinematic stage due to shear [25].

In conclusion, we have demonstrated via direct numerical simulations the presence of a novel second stage

growth of large-scale field, one that occurs between the kinematic stage driven by the SSD and the saturation stage driven by magnetic helicity decay. The SSD provides a seed for the LSD as postulated previously [26]. Interestingly, we find that this second stage of large-scale field growth sets in when the SSD slows down. Our detailed analysis reveals the important result that the classical mean-field theory applies well to understanding the large-scale field characteristics including its growth rate and frequency of oscillations. Moreover, the growth of the large-scale field in this second stage is independent of R_M. A major difficulty in the application of dynamo theory to large R_M systems like galaxies has been whether large-scale fields can grow at all in the presence of the SSD? However, our result now shows that exponential growth of fields by SSD is followed by an exponential growth of the large-scale field by LSD, thus indeed making it feasible to obtain large-scale fields on fast dynamical time-scales. Our work thus gives the first detailed evidence for how a large-scale dynamo operates quasi-kinematically once the small-scale field has saturated and develops an identity even amidst strong small-scale fields.

[1] A. P. Kazantsev, JETP **53**, 1807 (1967), (English translation: Sov. Phys. JETP, 26, 1031–1034, 1968).

[2] R. M. Kulsrud and S. W. Anderson, ApJ **396**, 606 (1992).

[3] S. I. Vainshtein and F. Cattaneo, ApJ **393**, 165 (1992).

[4] K. Subramanian and A. Brandenburg, MNRAS **445**, 2930 (2014), arXiv:1408.4416.

[5] P. Bhat, K. Subramanian, and A. Brandenburg, MNRAS **461**, 240 (2016), arXiv:1508.02706.

[6] A. Brandenburg, ApJ **550**, 824 (2001), astro-ph/0006186.

[7] DOI:10.5281/zenodo.2315093, github.com/pencil-code.

[8] H. K. Moffatt, *Magnetic Field Generation in Electrically Conducting Fluids* (Cambridge University Press, Cambridge, 1978).

[9] T. Elperin, N. Kleeorin, and I. Rogachevskii, PRE **68**, 016311 (2003), astro-ph/0301264.

[10] P. J. Käpylä, D. Mitra, and A. Brandenburg, PRE **79**, 016302 (2009), arXiv:0810.0833.

[11] P. J. Käpylä and A. Brandenburg, ApJ **699**, 1059 (2009), arXiv:0810.2298.

[12] C. Guervilly, D. W. Hughes, and C. A. Jones, Journal of Fluid Mechanics **815**, 333 (2017), arXiv:1607.00824 [physics.flu-dyn].

[13] N. K. Singh, I. Rogachevskii, and A. Brandenburg, ApJ **850**, L8 (2017), arXiv:1610.07215 [astro-ph.SR].

[14] A. Brandenburg and K. Subramanian, PhR **417**, 1 (2005a), arXiv:astro-ph/0405052.

[15] See Supplemental Material, which includes Refs. [10-11], regarding the suppression of the vorticity dynamo by the magnetic field.

[16] S. Sur, A. Brandenburg, and K. Subramanian, MNRAS **385**, L15 (2008), arXiv:0711.3789.

[17] A. Brandenburg, A. Bigazzi, and K. Subramanian, MNRAS **325**, 685 (2001), astro-ph/0011081.

[18] E. G. Blackman and A. Brandenburg, ApJ **579**, 359 (2002), astro-ph/0204497.

[19] See Supplemental Material for details of the evolution of the large and small-scale helicity.

[20] A. Hubbard, M. Rheinhardt, and A. Brandenburg, A&A **535**, A48 (2011), arXiv:1102.2617 [astro-ph.SR].

[21] See Supplemental Material, which includes Ref. [20], regarding a demonstration of mode switching.

[22] P. J. Käpylä, M. J. Korpi, and A. Brandenburg, A&A **491**, 353 (2008), arXiv:0806.0375.

[23] K. Subramanian, MNRAS **294**, 718 (1998), astro-ph/9707280.

[24] S. M. Tobias and F. Cattaneo, Natur **497**, 463 (2013).

[25] G. Nigro, P. Pongkitiwanichakul, F. Cattaneo, and S. M. Tobias, MNRAS **464**, L119 (2017).

[26] R. Beck, A. D. Poezd, A. Shukurov, and D. D. Sokoloff, A&A **289**, 94 (1994).

Supplemental Material

to "Efficient quasi-kinematic large-scale dynamo as the small-scale dynamo saturates"

by P. Bhat, K. Subramanian & A. Brandenburg

A. Shear helical dynamo: large-scale flows and late time behavior

We mentioned in the main paper that a large-scale component arises in the velocity field. This is shown in Fig. 7(a). The large-scale flow is seen to arise early on, just after the end of phase I, at $t = 100$. This is
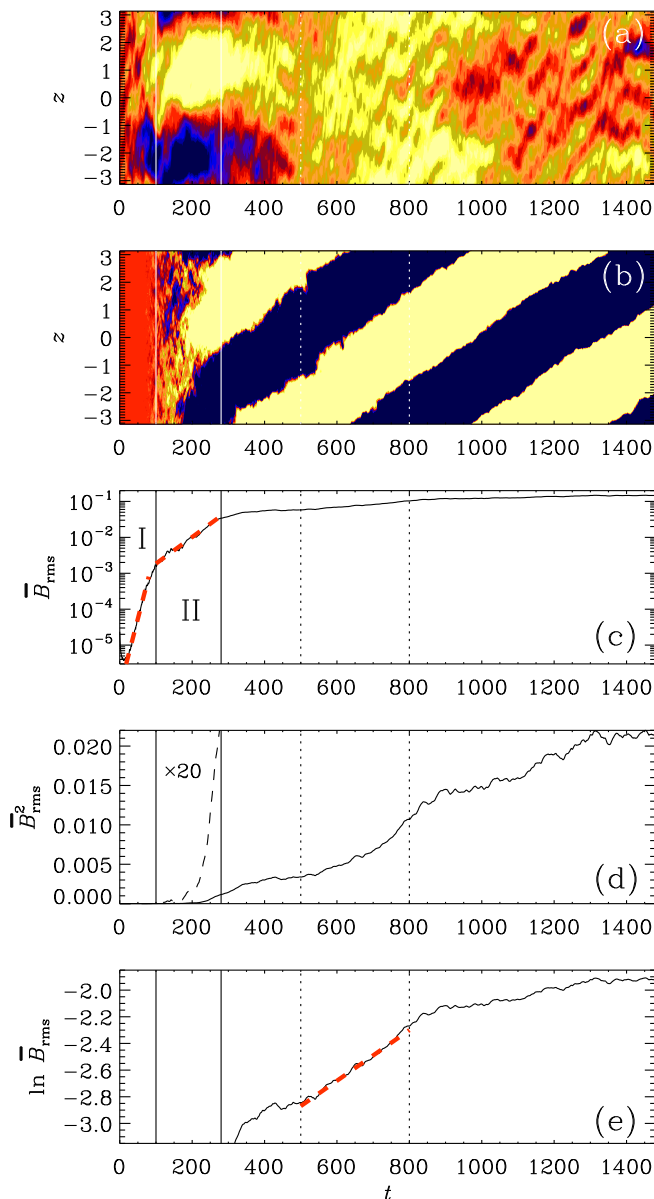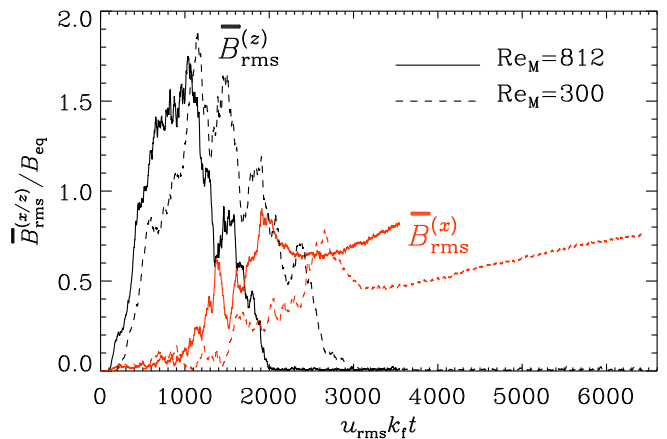

FIG. 8. Comparison of the rms values of the z dependent (xy-averaged, black lines) and x dependent (yz-averaged, red lines) mean fields, $\overline{B}^{(z)}_{\rm rms}$ and $\overline{B}^{(x)}_{\rm rms}$, respectively, for Run A (solid line) and a similar one at $R_M = 300$ (dotted lines).

due to a vorticity dynamo [9] and arises also without magnetic field [10]. Note that, because the large-scale flow varies only along the z direction, the relevant terms in the mean-field dynamo equation basically go to zero and thus this large-scale flow is not responsible for any magnetic field generation. At $t = 400$, the large-scale flow weakens, changes its form, and disappears by $t = 1000$. This suppression is due to the magnetic field [11, 12]. Figure 7(b) shows that a dynamo wave begins to emerge at $t = 100$, but it has initially a larger phase speed than at later times. In Fig. 7(c), we see that there is exponential growth in phases I and II with different growth rates. Figure 7(d) shows that this growth of $\overline{B}^2_{\rm rms}$ does not grow linearly in time. There is also evidence for another period of exponential growth at later times after phase II; see Fig. 7(e). The growth rate however is very slow and this perhaps arises due to a temporary fluctuation during the resistive phase.

As mentioned in the main paper, a fourth stage involves fratricide of this $\alpha\Omega$ dynamo by its α^2 sibling [20]. This can be seen by plotting the x dependent (yz-averaged) mean field, which we denote by $\overline{B}^{(x)}_{\rm rms}$ with superscript (x). The usual z dependent (xy-averaged) mean field is now denoted by $\overline{B}^{(z)}_{\rm rms}$ with superscript (z). This fratricide happens at much later times during $u_{\rm rms}k_{\rm f}t = 1000$–$2000$; see Fig. 8, where the black solid curve of $\overline{B}^{(z)}_{\rm rms}$ shows decay and simultaneously, $\overline{B}^{(x)}_{\rm rms}$ in solid red is growing. Importantly, it appears that the phase II is not R_M dependent as seen by comparing the near parallel solid and dashed black lines in Fig. 8 between $t = 100$ to 400. Thus, there is no evidence for catastrophic quenching of this phase in this range of R_M explored.
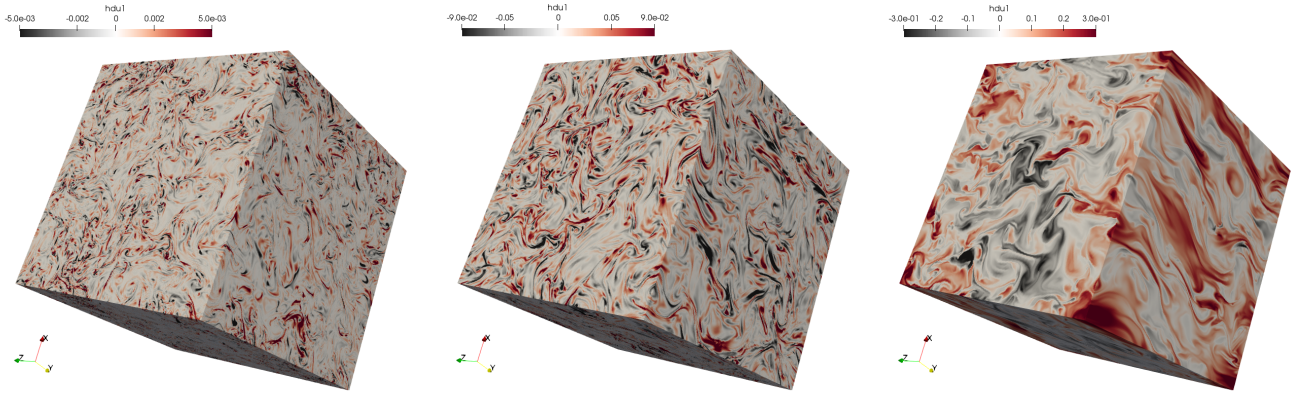

FIG. 7. Comparison of $\overline{u}_y$, $\overline{B}_y$, and three representations of $\overline{B}_{\rm rms}$ for Run A. The dotted line is scaled by $\times 20$.

FIG. 9. B_y for Run A at $t = 50, 200$ and 400.

B. Spatial organization of the field

To understand how the magnetic field changes in different stages of growth, we show in Fig. 9 the magnetic field component B_y of Run A at times $t = 50, 200$ and 400. At $t = 50$, the system is in kinematic stage and thus the fields are of small-scale nature. At $t = 200$, the large-scale dynamo (LSD) is active and one finds that the fields have started ordering themselves on larger and larger scales. In the third stage of resistive decay of helicity, the fields become increasingly organized and at $t = 400$, there is a coherent field on the largest scale in the box.

C. Magnetic helicity evolution in the dynamo with shear and helical forcing

In the main paper we mentioned that the build up of small-scale helicity during the second stage is expected to eventually quench the LSD. Initially, the LSD due to α-effect results in a helical polarization of the field, which is of opposite signs on small and large scales. The Lorentz force associated with this small scale helical field can back react to then quench the α-effect [6, 14, 17, 18]. Moreover, the large-scale field growth, which as discussed in the main paper is similar in helical and non-helical runs during the first stage when the SSD dominates, can however be differentiated at later stages by its helicity properties. Thus, it is of interest to examine the magnetic helicity power spectrum $H(k)$ for this standard signature of the LSD and study how it evolves in the first two stages of large-scale field growth discussed in the main paper.

In the kinematic stage, when the SSD is dominant, there is no clear separation between the positively helical and the negatively helical fields as shown by $H(k)$ in Fig. 10 for Run A. However, towards the end of the second stage (the curve at $t = 250$), a clear separation in scales based on helicity develops, i.e., the helicity on

smaller k, $k < k_{\rm f}$ is one sign represented by blue diamonds and the helicity on larger k is the opposite sign represented by red squares. It is this accumulation of small-scale helicity that could induce a magnetic back reaction to the initial kinetic α-effect and quench the LSD such that the exponential growth of the large-scale field transits to a resistively limited growth in the third stage.
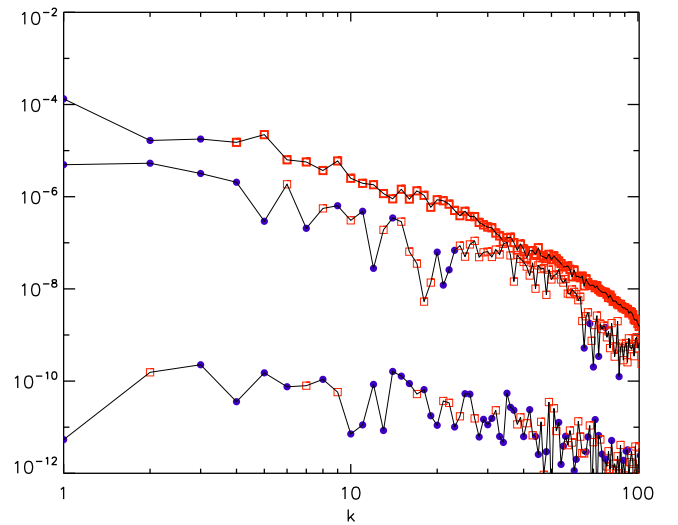

FIG. 10. The magnetic helicity power spectrum is shown at three times, $t = 100, 150$ & 250 for Run A. The blue diamonds represent negative helicity and red squares represent positive helicity.

At late times, when the α^2 dynamo is operating, magnetic helicity continues to build up at larger scales; see Fig. 11(a). Here, $H_\pm(t) = \int_\pm H(k,t)\,dk$, where $\int_\pm$ denote the integrals separately for positive and negative arguments, respectively. The gradual build-up of $H_-(t)$ happens by dissipating magnetic helicity of positive sign at small scales. The dissipation of $H_+(t)$ is proportional to the corresponding current helicity, $C_+(t)$, where $C_\pm(t) = \int_\pm k^2 H(k,t)\,dk$ are the contributions from positive and negative current helicity, respectively. Even-
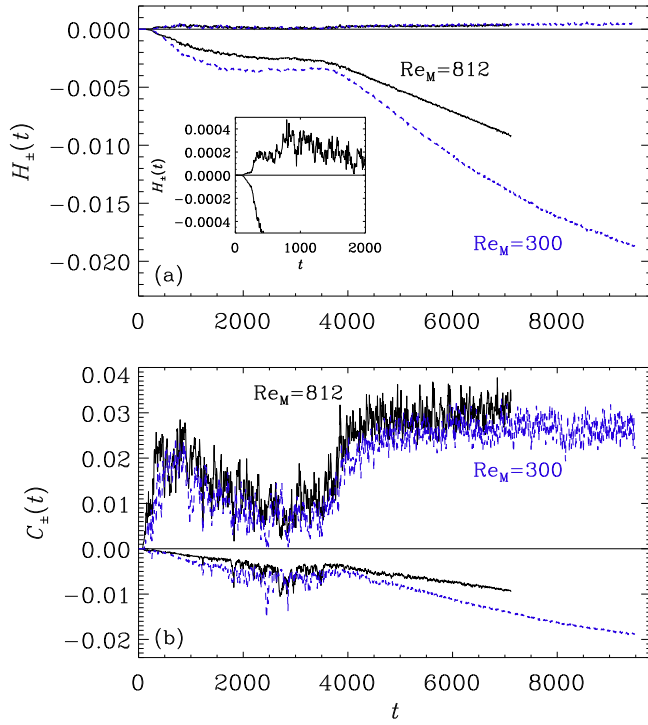
FIG. 11. Evolution of (a) $H_\pm(t)$ and (b) $C_\pm(t)$ for Run A and a similar run with $R_M = 300$. The inset highlights the early growth of $H_+(t)$.

tually, C_+ and C_-, begin to cancel each other; see Fig. 11(b). This leads to the asymptotic steady state where the total current helicity goes to zero and the large-scale field goes to the box scale as in [6]. Note this late time behaviour only occurs on the long resistive time scales.